Catalysis Today 155 (2010) 84–91

Contents lists available at ScienceDirect

Catalysis Today

journal homepage: www.elsevier.com/locate/cattod

Catalytic partial oxidation of a diesel surrogate fuel using an Ru-substituted pyrochlore

Daniel J. Haynes [a,b,c,*], Andrew Campos [c,1], David A. Berry [a,2], Dushyant Shekhawat [a,3], Amitava Roy [d,4], James J. Spivey [c,5]

[a] U.S. Department of Energy, National Energy Technology Laboratory, 3610 Collins Ferry Rd., Morgantown, WV 26507, United States
[b] Parsons, P.O. Box 618, South Park, PA 15129, United States
[c] Louisiana State University, Department of Chemical Engineering, 110 South Stadium Dr., Baton Rouge, LA 70803, United States
[d] J. Bennett Johnston Sr., Center for Advanced Microstructures and Devices, 6980 Jefferson Hwy., Baton Rouge, LA 70806, United States

ARTICLE INFO

Article history:
Available online 12 May 2009

Keywords:
Partial oxidation
Reforming
Ruthenium
Pyrochlore
Fuel processing
Diesel

ABSTRACT

Results from previous studies [D.J. Haynes, D.A. Berry, D. Shekhawat, J.J. Spivey, Catal. Today, doi:10.1016/j.cattod.2008.05.014; D.J. Haynes, D.A. Berry, D. Shekhawat, J.J. Spivey, Catal. Today 136 (2008) 206–213] show that Rh metal (2 wt%) substituted into a lanthanum–strontium–zirconate pyrochlore is highly active for the CPOX of surrogate diesel fuel compounds and their mixtures into synthesis gas for fuel cells. However, availability and cost of Rh suggests that it may not be optimal for widespread commercialized applications, and that other, cheaper metals should be investigated. To that end, a potentially lower cost ruthenium substituted pyrochlore catalyst (LSRuZ) was compared to a traditional supported Ru/γ-Al_2O_3 catalyst in the partial oxidation of a diesel surrogate fuel. Characterization results from XRD showed that the pre- and post-CPOX samples of LSRuZ catalysts consisted of two phases—the main $La_2Zr_2O_7$ pyrochlore phase as well as a defect $SrZrO_3$ perovskite phase. TPR results demonstrated that Ru atoms substituted into the pyrochlore structure were accessible to the gas-phase and were reducible. The substituted Ru had a higher reduction temperature compared to Ru/γ-Al_2O_3 (53 °C increase), likely due to interaction with neighboring metal ions in the pyrochlore. XANES spectra on substituted Ru showed the majority of Ru was in the 4+ oxidation state (but not in the RuO_2 phase) and was more likely substituted in the pyrochlore than the perovskite phase. Activity testing demonstrated that both catalysts produce equilibrium yields during initial 1 h CPOX of *n*-tetradecane only. However, after addition of 5 wt% 1-methylnaphthalene and dibenzothiophene to the feed, Ru/γ-Al_2O_3 deactivated immediately and was unable to recover activity once the contaminants were removed from the feed (irreversible deactivation). Conversely, the yields of LSRuZ dropped slightly, but remained steady over the 2 h when the contaminants were present, and almost recovered to pre-contaminant levels when the contaminants were removed. Carbon formation was directly linked to loss of activity. Post-run temperature programmed oxidation results showed that Ru/γ-Al_2O_3 had significantly more carbon on/around the active metal compared to the LSRuZ.

1. Introduction

The combustion of fossil fuels (i.e. coal, petroleum and natural gas) is the primary source of power production in transportation and stationary power applications in the U.S. [3]. However, combustion is relatively inefficient compared to advanced processes, due to significant heat and frictional losses during the conversion process [4]. Furthermore, the products of combustion, including NO_x, SO_x, particulate matter, CO, and CO_2, are the subject of current and anticipated regulations. There is therefore an interest in energy conversion technologies that utilize fossil fuel resources more efficiently with less environmental impact.

One effective means of using fossil fuels as an energy source is to catalytically reform them into synthesis gas (H_2 + CO), which

* Corresponding author at: U.S. Department of Energy, National Energy Technology Laboratory, 3610 Collins Ferry Rd, Morgantown, WV 26507, United States. Tel.: +1 304 285 1355; fax: +1 304 285 0903.
E-mail addresses: Daniel.Haynes@pp.netl.doe.gov (D.J. Haynes), Acampo2@lsu.edu (A. Campos), David.Berry@netl.doe.gov (D.A. Berry), Dushyant.Shekhawat@netl.doe.gov (D. Shekhawat), Reroy@lsu.edu (A. Roy), jjspivey@lsu.edu (J.J. Spivey).
[1] Tel.: +1 225 578 7032.
[2] Tel.: +1 304 285 4430.
[3] Tel.: +1 304 285 4634.
[4] Tel.: +1 225 578 6706.
[5] Tel.: +1 225 578 3690.

0920-5861/$ – see front matter © 2009 Elsevier B.V. All rights reserved.
doi:10.1016/j.cattod.2009.03.025

can then be converted to electrical power in a solid oxide fuel cell (SOFC). Of the available alternative technologies, no other energy production method offers the combination of clean energy and efficiency provided by an SOFC. Because a wide range of fuels can be used, SOFCs have proven to be versatile, and can be used in such applications as auxiliary power units (APUs) for diesel trucks, as well as decentralized stationary power for commercial and military applications.

Three main catalytic reforming reactions can be used to convert hydrocarbon fuels into synthesis gas (H_2 + CO) for fuel cells: steam reforming (SR), catalytic partial oxidation (CPOX), and autothermal reforming (ATR).

$$\text{SR}: \quad C_nH_m + H_2O \rightarrow H_2 + CO, \quad \Delta H > 0$$
$$\text{CPOX}: \quad C_nH_m + O_2 \rightarrow H_2 + CO, \quad \Delta H < 0$$
$$\text{ATR}: \quad C_nH_m + H_2O + O_2 \rightarrow H_2 + CO, \quad \Delta H \sim 0$$

The choice of the reforming reaction depends on the application. For the particular applications listed above for an SOFC, CPOX is generally considered to be the most practical because of its fast light-off capabilities and kinetics, which gives it a greater dynamic response to transients as well as high throughput. In addition, CPOX requires no added water, which is not readily available in remote locations.

A wide variety of hydrocarbons can be reformed to produce synthesis gas, including natural gas, coal, gasoline, and diesel. Of these fuels, diesel is the most practical choice in many cases, because it has the highest hydrogen energy density compared to other fuels [5] and a well-developed distribution infrastructure. However, it is also the most difficult fuel to reform because diesel fuel is a mixture of a wide variety of paraffin, naphthene, aromatic, and organosulfur compounds, each of which reacts differently in a CPOX reaction sequence. The specific nature of each of these components, i.e. chain length of *n*-paraffins, substituents attached to hydrocarbon rings, and degree of saturation of aromatic compounds affects the overall fuel conversion [6,7]. Some of these constituents are also known to deactivate reforming catalysts through carbon formation and sulfur poisoning [8].

Thus, the challenge in reforming diesel is to develop a catalyst that can maintain high product selectivity to H_2 and CO in the presence of aromatics and sulfur species, while being robust enough to operate at CPOX conditions, typically 800–1000 °C. Previous work has shown that certain metal oxides, such as hexaaluminates [9] and pyrochlores [1,2], can be used to prepare thermally stable catalysts. These oxides are of particular interest because catalytically active metals can be substituted within the structure of these materials to produce a thermally stable catalyst that resists both sulfur poisoning and carbon deposition [1,2,9]. Of particular interest is recent work on $La_{(2-x)}Sr_xRh_yZr_{(2-y)}O_{(7-\xi)}$ [1,2,10]. As prepared, this material showed both the pyrochlore and perovskite phases by XRD, and had superior resistance to deactivation by sulfur, aromatics, and carbon deposition compared to directly comparable formulations without Sr and/or Rh [1,2,10].

Rh metal was chosen for these studies [1,2,10] because it has been identified as the optimal catalyst for CPOX of logistic fuels. It has shown a high selectivity toward H_2 and CO [11–13] with lower carbon formation compared to other metals [14–16]. However, the cost of Rh, and its low nominal dispersion in these recent studies (ca. 5%) [1,2,10], suggest that other catalytically active metals should be investigated.

As an alternative, Ru would be an appropriate candidate—it is far less expensive than Rh, and its similar ionic radius and electronic properties (see Table 1) suggests that it could be substituted within the pyrochlore/perovskite structure. Moreover, Ru has been shown to improve the reforming properties of a non-catalytic perovskite material after incorporation into the structure. Liu and Krumpelt [17] demonstrated improved catalytic activity, in terms of increased H_2 and CO yields, of a partially substituted of Ru perovskite ($La_{0.8}Sr_{0.2}Cr_{0.95}Ru_{0.05}O_3$) during the ATR of a surrogate diesel fuel blend containing 500 ppmw sulfur.

Table 1
Elemental properties of Ru and Rh metals.

	Ru	Rh
Ionic radius (Å) (+4 valence and 6-fold coordination)	0.62	0.60
Electronegativity	2.20	2.28
Atomic electron affinity (eV)	1.05	1.14
1st ionization potential (eV)	7.37	7.46

*Values obtained from elemental database in HSC Chemistry software package [18].

No relevant studies in the literature have been found regarding the partial substitution of Ru into a pyrochlore structure, however it has been observed by Ashcroft et al. [19–22] that bulk ruthenate pyrochlores ($Ln_2Ru_2O_7$: Ln is a lanthanide) are highly active for both dry reforming and CPOX of methane. At an O/C = 1, 777 °C, and GHSV of 40,000 h^{-1} a $Pr_2Ru_2O_7$ pyrochlore had selectivities to H_2 and CO of 98% and 95%, respectively [19]. However, despite high activity, post-run characterization of this catalyst with XRD, XPS, and HRTEM revealed that the bulk Ru pyrochlore was not stable under CPOX conditions. Catalytic activity of the material was derived from the decomposition of the pyrochlore phase under the reducing reaction conditions, which created a Ru-metal enriched surface and a defect fluorite structure in the bulk due to the decreased Pr:Ru ratio. Decomposition was also observed on the ruthenate catalysts used for the CO_2 reforming of methane [20,21]. The structural instability of these materials is not desirable for reforming reactions like CPOX. During the breakdown of the pyrochlore structure, Ru migration to the surface leads to the formation of a supported metal catalyst, which should be avoided due to the increased tendency towards deactivation by carbon and sulfur [1,2].

The stability of Ru in the pyrochlore structure may be improved by partially substituting the Ru metal into the structure of the more stable lanthanum–strontium–zirconate. However, it is not known whether lanthanum–strontium–zirconate partially substituted with Ru would be as active and robust as Rh as a CPOX catalyst.

The objective of the work reported here is to characterize and test the CPOX activity of a Ru-substituted pyrochlore. Using *n*-tetradecane (TD) as a representative component of diesel fuel, experiments were performed with added sulfur (as dibenzothiophene, DBT) and a representative polynuclear aromatic (1-methylnaphthalene, MN) to determine the catalysts activity/selectivity to syngas, as well as its resistance to deactivation. Results are compared to a commercial Ru/γ-Al_2O_3 (0.5 wt% Ru) catalyst.

2. Experimental

2.1. Catalyst synthesis

The Ru substituted pyrochlore catalyst was synthesized by a modified Pechini method [23]. The experimental procedure for this method is shown below in Fig. 1. 0.5 wt% Ru/γ-Al_2O_3 (obtained from Alfa Aesar) was used as a baseline catalyst in characterization and CPOX studies. Nominal catalyst compositions and metal loadings are presented in Table 2.

2.2. Catalyst characterization

Phase analysis of the powder samples was examined using the Powder Diffraction (XPD) beamline at the J. Bennett Johnston Sr., Center for Advanced Microstructures and Devices (CAMD) at Louisiana State University. Subsequent peak identification of the

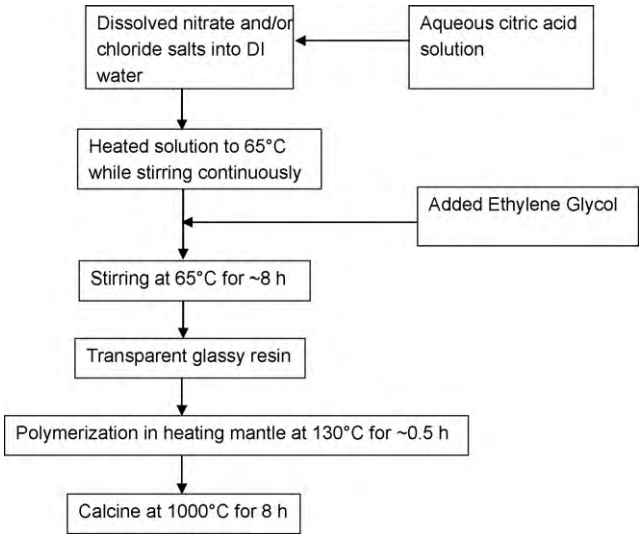

Fig. 1. Diagram of Pechini method [23] used to synthesize Ru metal oxide catalyst.

X-ray data was performed using X'pert High Score Plus software, version 2.1. Temperature programmed reduction (TPR) and H_2 pulse chemisorption experiments were performed in a Micromeritics Autochem 2910 unit. Experimental details for the TPR and H_2 pulse chemisorption experiments are specified in a previous study [2]. L_3-edge X-ray Absorption Near Edge Structure (XANES) studies of Ru substituted pyrochlore was taken at the Double Crystal Monochromator (DCM) beamline at CAMD using InSb(1 1 1) crystals. The operating energy of CAMD is 1.3 GeV, with a typical ring current between 100 and 200 mA. The DCM beamline, which has an approximate resolution of 0.5 eV at the energy range in this study, was calibrated with Ar gas (3.202 keV, 60 Torr) for the Ru L_3-edge. Ru standards used in the analysis were: RuO_2 (99.9% metals basis, Sigma–Aldrich), Ru^0 (−200 mesh, 99.9% metals basis, Alfa Aesar), and $RuCl_3$ (anhydrous, 99.9% metals basis, Alfa Aesar). The samples were placed on Kapton tape and scanned in fluorescence using a Vortex™ Si drifts detector (50 mm^2 active area) and a pressure of 3 Torr (of ambient air) was maintained during the scan with scanning parameters given in Table 3. L_3-edge of Ru in LSRuZ was compared to the *ab initio* calculated spectrum using FEFF 8.4 to determine crystal phase Ru would occupy in the pyrochlore structure [24].

2.3. Reaction studies

A detailed description of the reactor system is documented elsewhere [15]. Briefly, the catalytic tests were performed in a fixed-bed continuous-flow reactor (Autoclave Engineers, Model no. BTRS Jr). The catalyst was placed in an 8 mm i.d. tubular reactor and diluted with quartz sand (5 g silica per 1 g catalyst) of the same particle size as the catalyst, to minimize temperature gradients and channeling throughout the bed. Heat was supplied via a split-tube furnace, and the bed temperature was measured by an axially centered thermocouple. External heating was required to ensure a uniform temperature distribution throughout the catalyst bed. Although the CPOX reaction is highly exothermic, the reactant flow rates were too low for the reaction to sustain itself because of significant heat losses.

Table 2
Target catalyst compositions and active metal loadings.

	$La_{1.5}Sr_{0.5}Ru_{0.05}Zr_{1.95}O_{7-y}$ (LSRuZ)	Ru/γ-Al_2O_3
Metal loading (target wt%)	1.0	0.5[a]

[a] As obtained from Alfa Aesar.

Table 3
Scan parameters for Ru XANES.

Element (L_3-edge, keV)	Ru (2.838)
Scan interval (eV, rel. edge)	−50, −15, 30, 100
Step size (eV)	2, 0.2, 1
Integration time (s)	10

n-Tetradecane (TD), 1-methylnaphthalene (MN) and dibenzothiophene (DBT) were used to represent the major paraffin, aromatic, and sulfur compounds, respectively, that are commonly found in diesel fuels [6]. The experimental procedure involved three steps. First, the CPOX of TD only was conducted for 1 h to establish baseline activity and selectivity of the catalyst. Next, the feed was switched to 5 wt% MN and 50 ppmw DBT in TD for 2 h. Finally, the feed was switched back to TD only for 2 h to examine activity recovery. Experimental conditions are detailed below in Table 4. After CPOX experiments a temperature programmed oxidation (TPO) was performed to determine the amount of carbon deposited on the spent catalyst. The carbon was oxidized by passing a 5% mixture of O_2/N_2 over the catalyst while being heated from 200 to 900 °C at 1 °C/min.

The dry gas products: H_2, CO, CO_2, and N_2 were analyzed continuously by an online Thermo Onix mass spectrometer (Model no. Prima δb, a 200 amu scanning magnetic sector), while gaseous hydrocarbon products (C_1–C_6) were analyzed with an HP5890 gas chromatograph equipped with a flame ionization detector. Six GC samples were taken over the course of a 5 h experiment: the first at the beginning of the experiment (~ after 5 min), then one per hour as the experiment progressed. Carbon balances for all experiments were 100 ± 10%. Steam concentration was not measured analytically; however, it was estimated from mass balance calculations of hydrogen and oxygen-containing species in the product stream.

The following Eqs. (1)–(3) were used in the analysis of the experimental data. The yield of each dry gas product, i.e. H_2, CO, CO_2, and CH_4 was calculated by Eq. (1).

$$\text{Yield of } A\,(\%) = \frac{\text{Moles of } A \text{ produced} \times 100}{N \times \text{moles of TD fed to the reactor}} \quad (1)$$

where N is the number of moles of H_2 per mole of hydrocarbon for H_2 yields and is the number of moles of carbon in the hydrocarbon fuel for yields of carbon containing products.

Hydrocarbon (HC) yields were determined using Eq. (2).

$$\text{HC Yield}\,(\%) = \frac{\text{Moles of HC produced} \times i \times 100}{N \times \text{moles of TD fed to the reactor}} \quad (2)$$

where 'i' is the number of moles of carbon per mole of hydrocarbon in the product (i.e. i would be 2 for ethane) and 'N' is the number of moles of carbon in the hydrocarbon fuel.

A carbon balance was determined by Eq. (3).

$$\text{Carbon balance}\,(\%) = \frac{\left(\text{CO} + \text{CO}_2 + \sum_i^{i=1-6} i\text{C}_i\text{H}_r\right) \times 100}{N \times \text{moles of TD fed to the reactor}} \quad (3)$$

where i is the number of moles of carbon per mole of hydrocarbon in the product (i.e. i would be 2 for ethane), N is the number of

Table 4
Reaction conditions for CPOX experiments.

Reaction conditions	
O/C ratio	1.2
GHSV (scc g_{cat}^{-1} h^{-1})	50,000
Bed temperature (°C)	900
Catalyst bed (mg)	480
Pressure (MPa)	0.23

moles of carbon in the hydrocarbon fuel and '*r*' is the number of hydrogen atoms contained in the hydrocarbon product.

3. Results and discussion

3.1. Catalyst characterization

3.1.1. X-ray diffraction (XRD)

X-ray diffraction results of fresh and spent LSRuZ are shown below in Fig. 2. In the case of the fresh sample, no major phase changes in the bulk crystalline properties were observed after either Ru was substituted for the Zr^{4+} ions, indicating that the dopant metal is stable in the 6-fold coordination in the B-site. However, substitution of Sr^{2+} for La^{3+} results in a mixed phase crystalline structure, with a defect $SrZrO_3$ perovskite phase forming along with the main $La_2Zr_2O_7$ pyrochlore. The formation of the defect perovskite phase is consistent with a LSRhZ catalyst (2 wt% Rh) used in a previous study with the same Sr loading [10]. In addition, these results are consistent with other studies showing that Sr is only slightly soluble in zirconate pyrochlores, only up to 2.5 mol%, with the excess forming $SrZrO_3$ [25,26]. XRD pattern of the spent sample is almost identical to those of the fresh catalyst, indicating no major structural changes occurred during reaction.

3.1.2. Temperature programmed reduction (TPR)

TPR profiles for LSRuZ and Ru/γ-Al_2O_3 are presented in Fig. 3. The high temperature reduction peak (~555 °C) seen for LSRuZ is due to the reduction of the bulk pyrochlore structure [2]. The Ru/γ-Al_2O_3 shows two overlapping low temperature peaks (90 and 129 °C), which are due to the reduction of RuO_2 and other RuO_x species, respectively, to Ru metal [27].

Atomically dispersing Ru throughout the pyrochlore structure naturally reduces the amount of metal exposed at the surface because a significant portion of the metal is embedded in the bulk lattice. However, TPR profile of LSRuZ shows a low temperature peak that can be attributed to the reduction of Ru metal (182 °C), indicating some metal atoms are accessible to the gas phase and are reducible. As a result of substitution into the pyrochlore, Ru metal has an increase in reduction temperature of 53 °C compared to its γ-Al_2O_3 supported counterpart. This is probably due to the change in the neighboring ions surrounding the Ru atoms in the pyrochlore structure. The change in oxygen coordination of the Ru metal also likely increases the reduction temperature. When Ru is supported onto γ-Al_2O_3, the main phase consists of RuO_2 [27]. However, this changes when the metal occupies the B-site in the pyrochlore structure. In a fully developed pyrochlore crystal, Ru is coordinated with six oxygen atoms (RuO_6) [28]. However, since the reduction occurs at the surface, the metal ions there do not likely have this full coordination. Oxygen stoichiometries for surface Ru metal atoms could be RuO_{6-x}, (x = 0–5) which are different from the main metal oxide phase that exists on γ-Al_2O_3.

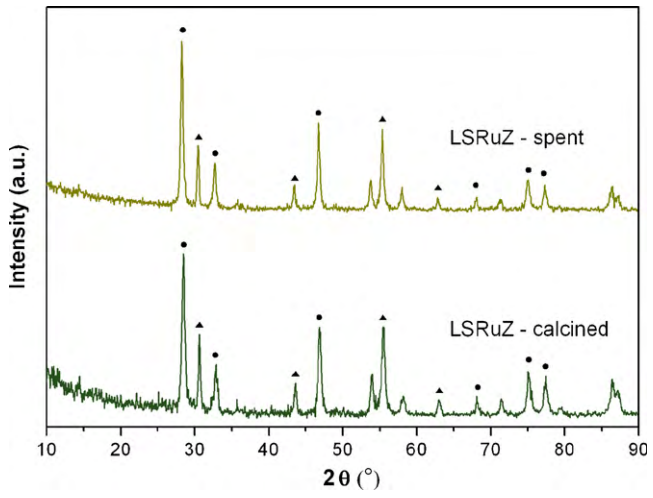

Fig. 2. XRD patterns for fresh and spent samples of LSRuZ. Peaks from $La_2Zr_2O_7$ pyrochlore (●); peaks from $SrZrO_3$ perovskite (▲).

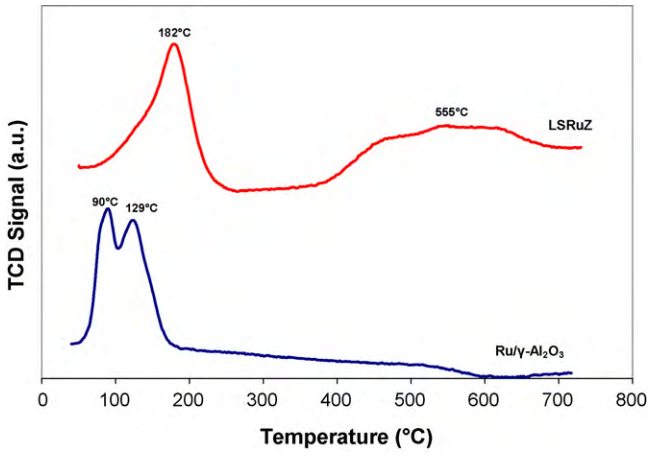

Fig. 3. TPR profiles for 0.5 wt% Ru/γ-Al_2O_3, and LSRuZ (1.0 wt% Ru).

Comparing the TPR profiles of LSRuZ and LSRhZ (2 wt% Rh) from a previous study [2] shows that, despite the different total nominal metal loading, substituted Ru is much more reducible than Rh. LSRuZ has a very large broad reduction peak centered at 182 °C, while LSRhZ has considerably smaller reduction peak centered at a much higher temperature of 274 °C.

The reduction peak at 182 °C for the LSRuZ (Fig. 3) is comparable to a peak at 150 °C observed by Liu and Krumpelt [17] for the $La_{0.8}Sr_{0.2}Cr_{0.95}Ru_{0.05}O_3$ perovskite (calcined at 800 °C) discussed earlier. The presence of a significant 150 °C TPR peak on their perovskite, coupled with EXAFS analysis, suggested that Ru was enriched at the surface under reducing conditions, presumably as extra framework or defect Ru. This is likely the case here as well. The shift in Fig. 3 for the RuO_x reduction peak from 90 to 120 °C for the Ru/γ-Al_2O_3, to 182 °C in the LSRuZ, shows that the surface Ru in the LSRuZ is more strongly oxidized than for either the Ru/γ-Al_2O_3, or the $La_{0.8}Sr_{0.2}Cr_{0.95}Ru_{0.05}O_3$ perovskite of Liu and Krumpelt.

3.1.3. H_2 pulse chemisorption

Metal dispersion, as measured by H_2 pulse chemisorption, is presented in Table 5. Ru/γ-Al_2O_3 shows a typical dispersion value for a metal supported on γ-Al_2O_3. Although pulse chemisorptions tests were performed on the Ru-pyrochlore, interpretation of the results is complicated by uncertainties about the metal-hydrogen stoichiometry, ensemble effects that can change the nature of the hydrogen adsorption site, electronic interactions between the active metal and surrounding atoms, as well as changes in adsorption kinetics due to structure sensitivity [29]. Each of these factors is altered by substituting the metal into the pyrochlore. Several studies [29–31] have shown specifically that the H_2 adsorption kinetics onto Ru crystallites supported on γ-Al_2O_3 can be significantly decreased through the addition of metals into the

Table 5
Amount of accessible metal atoms for Ru/γ-Al_2O_3, and LSRuZ catalysts.

	Accessible metal atoms (%)
Ru/γ-Al_2O_3 (0.5 wt% Ru)	27
LSRuZ (0.57 wt% Ru)	2.3

*All metal loadings are nominal values.

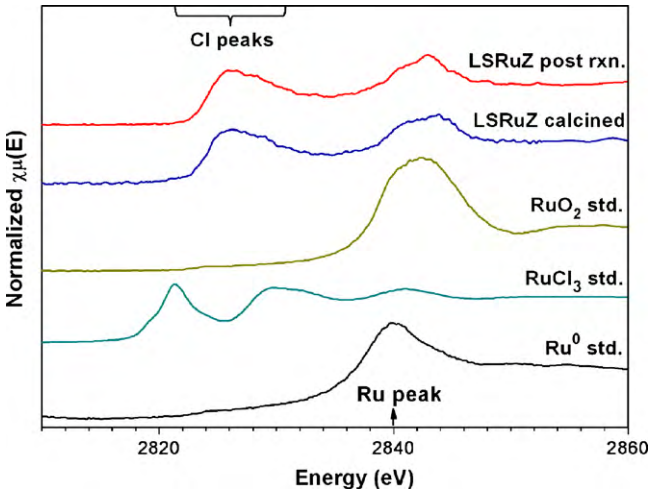

Fig. 4. Ru L_3-edge XANES of LSRuZ (fresh) calcined, post-reaction catalyst, and Ru^0, $RuCl_3$ (anhydrous), RuO_2 standards.

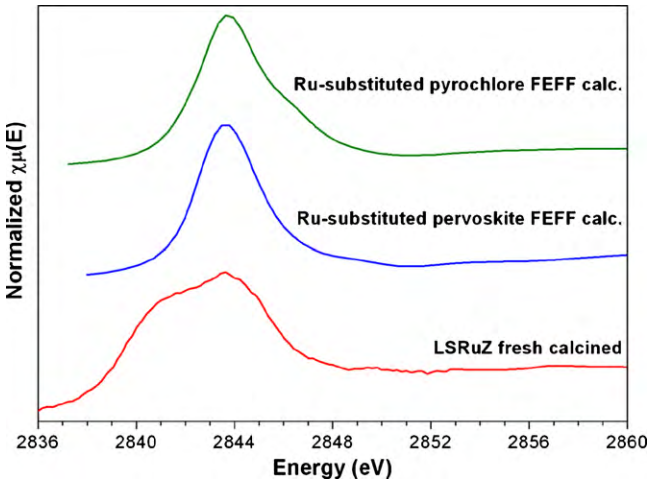

Fig. 5. FEFF 8.4 calculations for Ru in pyrochlore and perovskite structures compared with LSRuZ calcined spectrum.

lattice (Ag or Cs). For these reasons, the pulse chemisorption results for the Ru-pyrochlore cannot be compared directly to those for Ru/γ-Al_2O_3.

3.1.4. LSRuZ XANES

Fig. 4 shows the Ru L_3-edge XANES of the LSRuZ catalyst after calcination and reaction (which was followed by TPO up to 900 °C to remove carbon formed during reaction) as well as Ru^0, $RuCl_3$ (anhydrous), and RuO_2 standards. The first edge in Fig. 4 was identified as the Cl K-edge (2822 eV), since it was present in the $RuCl_3$ standard. This peak was observed in the LSRuZ catalyst after calcination and after reaction. Although thermodynamics suggest that residual Cl from the synthesis procedure would have been vaporized during the 1000 °C calcination step, the XANES shows that residual Cl was oxidized to the ClO_3^- anion [32]. A study by Kim et al. [33] suggested that the Cl contribution to the Ru L_3-edge is minor; other studies specific to the Cl K-edge show an approximately flat line in the Ru L_3-edge region corresponding to minimal peak overlap [32,34].

The edge-region for the Ru L_3-edge are transitions of $2p_{3/2} \rightarrow 4d_{5/2}$ and $4d_{3/2}$; in cases of octahedral symmetry (i.e. perovskite or pyrochlore) the width of the peak is sensitive to the oxidation state. For octahedral symmetry, two distinct peaks would indicate Ru^{5+}, and a single peak would indicate Ru^{4+} [34]. If Ru were in the 3+ oxidation state, the peak would have shifted to the left by ~0.9 eV (as shown in $RuCl_3$ spectrum) [34–36]. It was observed that the XANES spectrum of the LSRuZ catalyst was not shifted relative to RuO_2 suggesting that the majority of Ru was in the 4+ oxidation state [34]. A shoulder was observed in the LSRuZ XANES spectra, but was not present in the RuO_2 spectrum. This suggests that the majority of Ru present in the LSRuZ catalyst was substituted (likely for Zr-sites) to form a Ru-substituted pyrochlore or perovskite; FEFF calculations were used to determine which of the two phases were in better agreement with the data.

The L_3-edge of Ru^{4+}-containing species typically have a single peak, [34]; FEFF 8.4 calculations in Fig. 5 predicted a single major peak for Ru^{4+} in the pyrochlore and perovskite phase, which is consistent with the experimental data from the LSRuZ XANES spectrum. The wider peak predicted by the FEFF calculation of the Ru-containing pyrochlore indicates that is was in closer agreement with the data than for the Ru-substituted perovskite, suggesting that it is more probable that Ru in the LSRuZ catalyst was substituted into the pyrochlore phase.

3.2. CPOX results

3.2.1. Equilibrium and blank reactor

Equilibrium values for the CPOX of TD as well as results from the CPOX of TD in a blank reactor are presented in Table 6. This data is discussed more thoroughly in a previous study [2], and the summary below is provided here for reference.

3.2.2. CPOX of n-tetradecane

The yields produced over Ru/γ-Al_2O_3 and LSRuZ during the 5 h CPOX studies are shown in Figs. 6 and 7, respectively. During the initial 1 h of reforming TD only, the H_2 and CO yields of both Ru catalysts are essentially equilibrium values (Table 6). The comparable initial activity of Ru/γ-Al_2O_3 and LSRuZ indicates that the substitution of the Ru metal into the pyrochlore structure does not have a detrimental effect on the catalytic properties of the metal as measured at the CPOX conditions studied here. These yields are also comparable to those produced over LSRhZ (2 wt% Rh) and 0.5 wt% Rh/γ-Al_2O_3 catalysts during the CPOX of TD only [2].

3.2.3. Effects of aromatics and sulfur

The addition of 5 wt% MN and 50 ppmw DBT to the feed after 1 h on stream decreases the yields of CO and H_2 for all catalysts. Corresponding to this decrease in synthesis gas yields is an increase in olefin yields (Fig. 8).

Table 6
Equilibrium and blank reactor (quartz sand) product yields, and carbon balance for the CPOX of TD at O/C = 1.2, P = 0.23 MPa, 900 °C and 50,000 scc g_{cat}^{-1} h^{-1} [2].

	Equilibrium[a]	Quartz sand (blank)
H_2 yield (%)	90.0	17.0
CO yield (%)	92.0	42.0
CO_2 yield (%)	8.5	17.0
CH_4 yield (%)	0.1	8.0
Ethane yield (%)	0.0	0.7
Ethylene yield (%)	0.0	16.3
Propylene yield (%)	0.0	1.5
C_4-ene yield (%)	0.0	1.0
Benzene yield (%)	0.0	3.9
Carbon balance (%)	100	90

[a] Equilibrium calculations were made using a Gibb's minimization technique in HSC Chemistry Thermodynamic Software [37]. Calculations were made assuming a mixture of 2 mol% TD, 18 mol% O_2, and 80 mol% N_2.

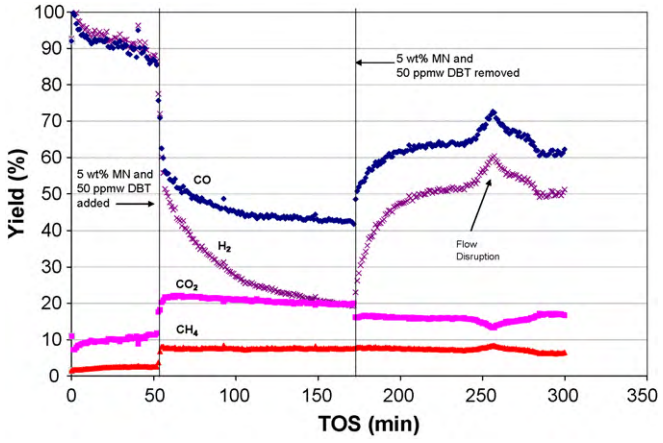

Fig. 6. Yields for Ru/γ-Al_2O_3 during 5 h CPOX experiment; O/C = 1.2, 0.23 MPa, 900 °C and 50,000 scc g_{cat}^{-1} h^{-1}. H_2 (×), CO (◆), CO_2 (■), and CH_4 (▲).

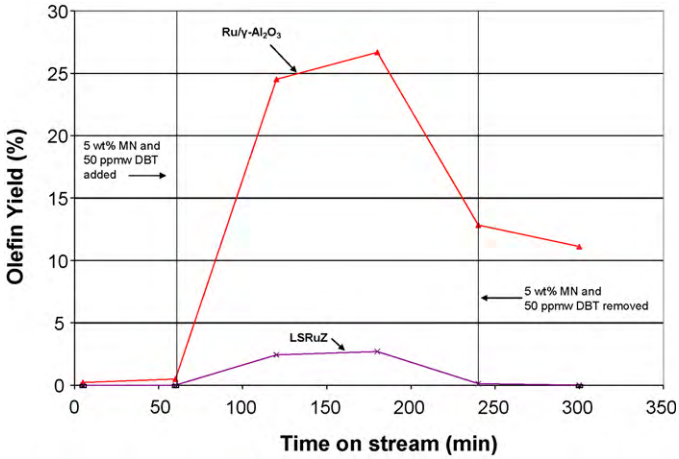

Fig. 8. Olefin yields for Ru/γ-Al_2O_3, and LSRuZ during 5 h CPOX experiment; O/C = 1.2, 0.23 MPa, 900 °C and 50,000 scc g_{cat}^{-1} h^{-1}. Ru/γ-Al_2O_3 (▲), and LSRuZ (×).

It can be seen from Figs. 6–8 that the MN and DBT have a more adverse effect on the Ru/γ-Al_2O_3 than the Ru-substituted pyrochlore. For the γ-Al_2O_3-supported catalyst, H_2 yields drop continuously over the 2 h the contaminants are in the feed, while CO yields also drop continuously, but at a much lower rate. After 2 h in the presence of the contaminants, H_2 and CO yields approach those of a blank reactor (Table 6) for the Ru/γ-Al_2O_3. This behavior has been observed previously for a 1.0 wt% Pt/γ-Al_2O_3, $Co_{0.4}Mo_{0.6}C_x$ carbide catalyst, and a 0.5 wt% Rh/γ-Al_2O_3 in the presence of 5 wt% MN/TD (no DBT) and 1000 ppmw DBT/TD (no MN) under the same conditions as those used in this study [10,38]. It has been speculated that this behavior was due to the deactivation of catalytic sites in the downstream portion of the bed, where the endothermic reforming reactions between the unreacted fuel fragments and $CO_2 + H_2O$ take place (all of which are likely to have formed near the inlet by combustion of fuel with available O_2) [38–40].

After the MN and DBT are removed from the feed H_2 and CO yields do not return to initial levels for the Ru/γ-Al_2O_3. Olefin yields remain high during the 2 h recovery period, indicating the surface of the catalyst has been deactivated and reactions are occurring in the gas-phase [40–42]. The fact that catalytic activity does not return to initial levels suggests that the MN and sulfur act as irreversible poisons to the supported metal catalyst, at least over the 2 h time scale studied here.

It has been found that the adsorption of carbon [43–45] and sulfur [9,46] is directly linked to the size of the metal ensembles on the surface; i.e. smaller sites will less easily adsorb carbon or sulfur than larger ones. The results here (Figs. 6–8) suggest that the Ru/γ-Al_2O_3 catalyst has sufficiently large ensembles of metal on the surface at reaction conditions to be easily poisoned.

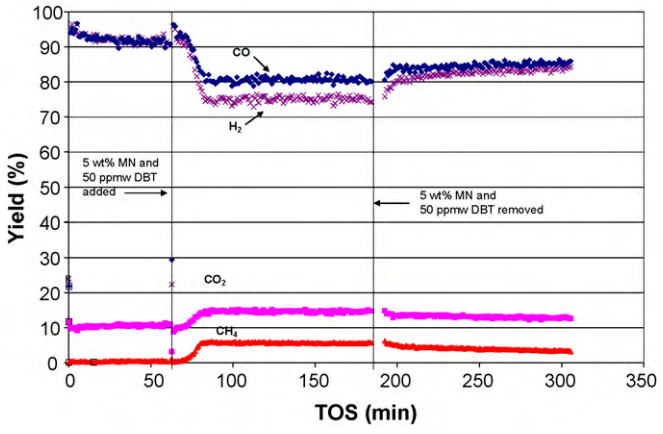

Fig. 7. Yields for LSRuZ during 5 h CPOX experiment; O/C = 1.2, 0.23 MPa, 900 °C and 50,000 scc g_{cat}^{-1} h^{-1}. H_2 (×), CO (◆), CO_2 (■), and CH_4 (▲).

There are two important effects of the substitution Ru into the pyrochlore structure. First, the presence of sulfur (DBT) and aromatics (MN) has a far less detrimental effect on H_2 and CO yields for the pyrochlores than the γ-Al_2O_3-supported catalyst (Figs. 6–8), possibly due to the absence of easily poisoned large metal ensembles. Second, unlike the γ-Al_2O_3 supported counterpart, the H_2 and CO yields for the LSRuZ do not decrease continuously in the presence of DBT and MN, but rather drop quickly to lower, but steady, levels. This is evidence of kinetic inhibition of the active catalytic sites by the contaminants rather than catalyst deactivation. Olefins remain low after DBT and MN are added (Fig. 8), indicating that the Ru in the pyrochlore structure is able to retain its catalytic activity in the presence of the contaminants.

After the contaminants are removed, the H_2 and CO yields for the LSRuZ recover, but do not reach initial levels, at least within the 2 h duration of the post-contaminant tests carried out here. However, the small but positive slope of the H_2 and CO yields for LSRuZ during the post-contaminant portion of the tests is consistent with kinetic inhibition caused by DBT and MN. Also note (Fig. 8) that olefin yields return to zero for the pyrochlore catalyst once the contaminants are removed.

Collectively, these results can be explained by the rapid (but limited) deposition of surface species derived from, or caused by, DBT and/or MN. These surface species limit the approach to equilibrium H_2 and CO yields on the pyrochlore, and do not continuously accumulate on the surface, but rather reach some steady state level at the conditions examined here. Further, the adsorption of these species is somewhat reversible, as the LSRuZ recovers to almost initial activity within 2 h. Given sufficient time, the results suggest that full initial activity would be restored.

Despite different metal loading and feed conditions (all other reaction conditions were the same), the LSRuZ (1 wt% Ru) appears to have comparable activity to the LSRhZ (2 wt% Rh) catalyst used in a previous study [10]. Both catalysts show promise as viable logistic fuel reforming catalysts as each were able to maintain high activity as well as selectivity during the CPOX of surrogate diesel fuel mixtures to synthesis gas: 5 wt% MN + 50 ppmw DBT/TD for LSRuZ; 5 wt% MN only/TD, 1000 ppmw DBT only/TD and 5 wt% MN + 1000 ppmw DBT/TD for LSRhZ.

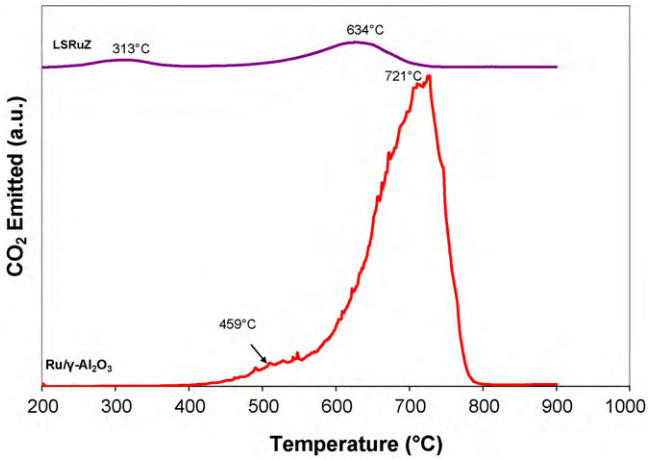

Fig. 9. TPO profiles from Ru/γ-Al_2O_3, and LSRuZ after 5 h CPOX study: CPOX TD only for 1 h, CPOX 5 wt% MN and 50 ppmw DBT/TD for 2 h, and CPOX TD only for 2 h; O/C = 1.2, 0.23 MPa, 900 °C and 50,000 scc g_{cat}^{-1} h^{-1}.

3.2.4. Carbon formation

Temperature programmed oxidation (TPO) profiles for each catalyst are presented in Fig. 9, and the corresponding amount of oxidizible carbon is shown in Table 7. The LSRuZ shows that far less carbon is deposited on the pyrochlore (0.07 $g_{carbon}/g_{catalyst}$) than on the Ru/γ-Al_2O_3 catalyst (0.60 for Ru/γ-Al_2O_3). This can be attributed to the presence of Sr in the pyrochlore structure, which creates structural defects that increase the oxygen-ion conductivity of the material [2]. This appears to greatly reduce the deposition of carbon on the catalyst.

Carbon formation on supported metal catalysts has been observed to form on three different parts of the surface: the metal, the metal-support interface and on the support [2,10,15,43,47]. The TPO profiles for the Ru/γ-Al_2O_3 catalyst shows two main identifiable peaks at 709 and 721 °C. This large peak overlaps a small, low temperature peak at 459 °C. These small low temperature shoulders (459 °C peak for Ru/γ-Al_2O_3) can be assigned to carbon formed on the metal [2,10,15,43,47]. The two main peaks (721 and 707 °C) occur near the temperature ranges that correspond to carbon formed at the metal-support interface [47].

TPO of the LSRuZ catalysts shows there are two small peaks on the catalyst—one at about 313 °C and one at roughly 634 °C. The low temperature peak ~313 °C is attributable to carbon on or near the surface metal atoms [2,15,43,47], while the ~634 °C peak is attributable to carbon on the oxide surface [2]. It is especially noticeable that more carbon deposited on/near the active metal sites for Ru/γ-Al_2O_3 in contrast to LSRuZ. Comparison of the peaks in which carbon has deposited on/near the metal (459 and 721 °C for Ru/γ-Al_2O_3 and 313 °C for LSRuZ in Fig. 9) shows that Ru has much greater carbon forming properties when supported on γ-Al_2O_3 compared to when it is substituted into the pyrochlore structure. This can likely explain why Ru/γ-Al_2O_3 had lower activity recovery when the contaminants were removed from the feed (Figs. 6 and 7) compared to the Ru-pyrochlore.

Table 7
Carbon deposited after 5 h CPOX study: CPOX TD only for 1 h, CPOX 5 wt% MN and 50 ppmw DBT/TD for 2 h, and CPOX TD only for 2 h; O/C = 1.2, 0.23 MPa, 900 °C and 50,000 scc g_{cat}^{-1} h^{-1}.

	Amount of carbon adsorbed ($g_{carbon}/g_{cat.}$)
0.5 wt% Ru/γ-Al_2O_3	0.60
LSRuZ (0.57 wt% Ru)	0.07

4. Conclusions

XRD results of pre- and post-run samples show that the LSRuZ catalyst consisted of two phases—the main $La_2Zr_2O_7$ pyrochlore phase as well as a defect $SrZrO_3$ perovskite phase. TPR results show that Ru-metal atoms substituted into the pyrochlore structure were accessible to the gas-phase and were reducible. The Ru XANES spectra showed the majority of Ru was in the 4+ oxidation state with octahedral symmetry (but not in the RuO_2 phase), and FEFF calculations indicated that it was more probable that it substituted into the pyrochlore than the perovskite phase. LSRuZ was only kinetically inhibited by the addition of 5 wt% MN and 50 ppmw DBT/TD to the feed, while Ru/γ-Al_2O_3 was irreversibly deactivated within 2 h to the point that the H_2 and CO yields approached those of a blank reactor. Activity did not return fully to equilibrium levels for the LSRhZ once the contaminants were removed from the feed; however, olefin yields did return to zero, suggesting that the kinetic inhibition was reversible. Temperature programmed oxidation results showed that the LSRuZ accumulated far less carbon formed on the surface compared to Ru/γ-Al_2O_3. This may be due to greater oxygen-ion conductivity properties of the Sr-containing pyrochlores. In addition, LSRuZ had less carbon formed on/near the active metal compared to Ru/γ-Al_2O_3. This suggests that deactivation of the γ-Al_2O_3-supported catalyst may have been due to carbon formed on active metal sites. From the results seen from this study, Ru can be substituted into the pyrochlore structure to create a less costly catalyst that resists deactivation by sulfur and aromatics, and which has activity comparable to the Rh-substituted pyrochlore.

Acknowledgements

This work was performed in support of the National Energy Technology Laboratory's on-going research in fuel processing, under contract # DE-AC26-04NT41817 subtask 41817.610.01.01. The authors would also like to gratefully acknowledge Donald Floyd for his invaluable contributions to this work in performing the experiments, and LSU's CAMD synchrotron facility for providing beam time.

References

[1] D.J. Haynes, D.A. Berry, D. Shekhawat, J.J. Spivey, Catal. Today, doi:10.1016/j.cattod.2008.05.014.
[2] D.J. Haynes, D.A. Berry, D. Shekhawat, J.J. Spivey, Catal. Today 136 (2008) 206–213.
[3] E.I.A., http://www.eia.doe.gov/emeu/aer/pdf/aer.pdf, Annual Energy Review, 2007, Accessed 01/2008.
[4] J. Larminie, A. Dicks, Fuel Cell Systems Explained, 2 ed., John Wiley & Sons Inc., West Sussex, 2003.
[5] C. Song, C.S. Hsu, I. Mochida, Chemistry of Diesel Fuels, Taylor and Francis, New York, 2000.
[6] D. Shekhawat, D.A. Berry, D.J. Haynes, J.J. Spivey, Fuel 88 (2009) 817–825.
[7] R. Subramanian, G.J. Panuccio, J.J. Krummenacher, I.C. Lee, L.D. Schmidt, Chem. Eng. Sci. 59 (2004) 5501–5507.
[8] D. Shekhawat, D.A. Berry, T.H. Gardner, J.J. Spivey, in: J.J. Spivey, K.M. Dooley (Eds.), Catalysis, The Royal Society of Chemistry, Cambridge, 2006, pp. 184–253.
[9] T.H. Gardner, D. Shekhawat, D.A. Berry, M.W. Smith, M. Salazar, E.L. Kugler, Appl. Catal. A 323 (2007) 1–8.
[10] D.J. Haynes, "The Catalytic Partial Oxidation of n-Tetradecane on Rh and Sr Substituted Pyrochlores", Master's Thesis, Louisiana State University, 2007.
[11] J.J. Krummenacher, L.D. Schmidt, J. Catal. 222 (2004) 429–438.
[12] J.J. Krummenacher, K.N. West, L.D. Schmidt, J. Catal. 215 (2003) 332–343.
[13] M. Huff, P.M. Torniainen, L.D. Schmidt, Catal. Today 21 (1994) 113–128.
[14] R.P. O'Connor, E.J. Klein, L.D. Schmidt, Catal. Lett. 70 (2000) 99–107.
[15] D. Shekhawat, T.H. Gardner, D.A. Berry, M. Salazar, D.J. Haynes, J.J. Spivey, Appl. Catal. A 311 (2006) 8–16.
[16] P.M. Torniainen, X. Chu, L.D. Schmidt, J. Catal. 146 (1994) 1–10.
[17] D.-J. Liu, M. Krumpelt, Int. J. Appl. Ceram. Technol. 2 (2005) 301–307.
[18] A. Roine, HSC Chemistry, 6.12 ed., Outotec Research Oy, Pori, Finland, 2007.
[19] A.T. Ashcroft, A.K. Cheetham, J.S. Foord, M.L.H. Green, C.P. Grey, A.J. Murrell, P.D.F. Vernon, Nature 344 (1990) 319–321.
[20] A.T. Ashcroft, A.K. Cheetham, R.H. Jones, S. Natarajan, J.M. Thomas, D. Waller, Catalysis and Surface Science Characterisation, vol. 114, Special Publication-Royal Society of Chemistry, 1992, pp. 184–189.

[21] A.T. Ashcroft, A.K. Cheetham, R.H. Jones, S. Natarajan, J.M. Thomas, D. Waller, S.M. Clark, J. Phys. Chem. 97 (1993) 3355–3358.
[22] R.H. Jones, A.T. Ashcroft, D. Waller, A.K. Cheetham, J.M. Thomas, Catal. Lett. 8 (1991) 169–174.
[23] M.P. Pechini, United States, Patent no. 3330697, 1963.
[24] A.L. Ankudinov, B. Ravel, J.J. Rehr, S.D. Conradson, Phys. Rev. B: Condens. Matter 58 (1998) 7565–7576.
[25] I. Hayakawa, H. Kamizono, J. Nucl. Mater. 202 (1993) 163–168.
[26] S.J. Patwe, A.K. Tyagi, Ceram. Int. 32 (2006) 545–548.
[27] R. Lanza, S.G. Järås, P. Canu, Appl. Catal. A 325 (2007) 57–67.
[28] M.A. Subramanian, G. Aravamudan, G.V.S. Rao, Prog. Solid State Chem. 15 (1983) 55–143.
[29] N. Kumar, T.S. King, R.D. Vigil, Chem. Eng. Sci. 55 (2000) 4973–4979.
[30] D.P. VanderWiel, M. Pruski, T.S. King, J. Catal. 188 (1999) 186–202.
[31] C. Zupanc, A. Hornung, O. Hinrichsen, M. Muhler, J. Catal. 209 (2002) 501–514.
[32] F.E. Huggins, G.P. Huffman, Fuel 74 (1995) 556–569.
[33] P.S. Kim, T.K. Sham, P. Zhang, M.K. Fung, S.T. Lee, Y.F. Hu, B.W. Yates, J. Am. Chem. Soc. 123 (2001) 8870–8871.
[34] J.-H. Choy, J.-Y. Kim, S.-H. Hwang, S.-J. Kim, G. Demazeau, Int. J. Inorg. Mater. 2 (2000) 61–70.
[35] I.C. Stefan, Y.B. Mo, M.R. Antonio, D.A. Scherson, J. Phys. Chem. B 106 (2002) 12373–12375.
[36] B.N. Lin, C.Y. Lin, Y.S. Wu, H.C. Ku, J. Magn. Magn. Mater. 272–276 (Pt. 1) (2004) 479–481.
[37] A. Roine, HSC Chemistry, 4.0 ed., Outkumpu Research Oy, Pori, Finland, 1999.
[38] D.J. Haynes, D.A. Berry, D. Shekhawat, T.-C. Xiao, M.L.H. Green, J.J. Spivey, Ind. Eng. Chem. Res. 47 (2008) 7663–7671.
[39] G.J. Panuccio, L.D. Schmidt, Appl. Catal. A 332 (2007) 171–182.
[40] M.C. Huff, I.P. Androulakis, J.H. Sinfelt, S.C. Reyes, J. Catal. 191 (2000) 46–54.
[41] E. Ranzi, M. Dente, A. Goldaniga, G. Bozzano, T. Faravelli, Prog. Energy Combust. Sci. 27 (2001) 99–139.
[42] A. Beretta, E. Ranzi, P. Forzatti, Chem. Eng. Sci. 56 (2001) 779–787.
[43] J. Barbier, Appl. Catal. 23 (1986) 225–243.
[44] J. Barbier, G. Corro, Y. Zhang, Appl. Catal. 13 (1985) 245–255.
[45] O. Yamazaki, K. Tomishige, K. Fujimoto, Appl. Catal. A 136 (1996) 49–56.
[46] J. Barbier, P. Marecot, L. Tifouti, M. Guenin, R. Frety, Appl. Catal. 19 (1985) 375–385.
[47] A. Shamsi, J.P. Baltrus, J.J. Spivey, Appl. Catal. A 293 (2005) 145–152.